ACS OMEGA

http://pubs.acs.org/journal/acsodf

Article

Highly Impact-Resistant Block Polymer-Based Thermoplastic Elastomers with an Ionically Functionalized Rubber Phase

Takato Kajita, Atsushi Noro,* Ryoji Oda, and Sadaharu Hashimoto

Cite This: *ACS Omega* 2022, 7, 2821−2830

Read Online

ACCESS | Metrics & More | Article Recommendations | Supporting Information

ABSTRACT: There has been a great deal of interest in incorporating noncovalent bonding groups into elastomers to achieve high strength. However, the impact resistance of such elastomers has not been evaluated, even though it is a crucial mechanical property in practical usage, partly because a large-scale synthetic scheme has not been established. By ionizing the rubber component in polystyrene-*b*-polyisoprene-*b*-polystyrene (SIS), we prepared several tens of grams of SIS-based elastomers with an ionically functionalized rubber phase and a sodium cation (i-SIS(Na)) or a bulky barium cation (i-SIS(Ba)). The i-SIS(Na) and i-SIS(Ba) exhibited very high tensile toughness of 520 and 280 MJ m^{-3}, respectively. They also exhibited excellent compressive resistance. Moreover, i-SIS(Ba) was demonstrated to have a higher impact resistance, that is, more protective of a material being covered compared to covering by typical high-strength glass fiber-reinforced plastic. As such elastomers can be produced at an industrial scale, they have great market potential as next-generation elastomeric materials.

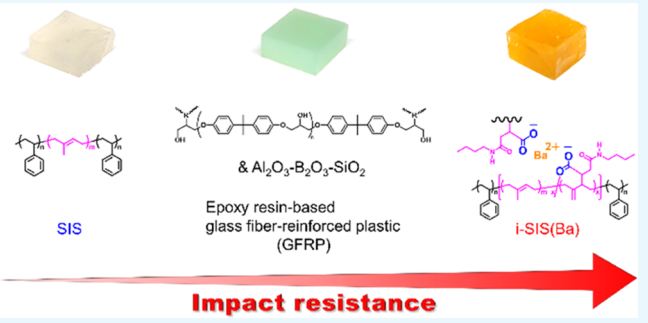

1. INTRODUCTION

Polymers that consist of many monomers connected by covalent bonds are widely used as polymeric materials (e.g., plastics, rubbers, polymer gels, fibers) in our daily life.[1] In particular, polymeric materials with a glass-transition temperature (T_g) or melting point (T_m) higher than room temperature are used as plastics; these include polystyrene, poly(vinyl chloride), polyethylene, and polypropylene. Although plastics are typically weaker than metals, they are lighter due to lower densities; therefore, plastics are often used as lightweight structural materials that replace heavy metals.

In recent years, as material applications have become more diverse and complex, the demand has grown for high-performance polymeric materials, thus leading to extensive studies on compounding polymeric materials, i.e., polymer composites.[2,3] Examples of well-known polymer composites include fiber-reinforced plastics (FRPs).[4,5] FRPs are extremely high-strength composite materials consisting of a thermosetting resin, such as an epoxy resin, or a thermoplastic, such as polypropylene, with high-strength fibers, such as glass fibers or carbon fibers. FRPs also exhibit excellent impact resistance because they comprise a resin or thermoplastic that can be easily deformed compared to high-strength fibers.[6]

The above-mentioned polymer composites are macroscopically compounded materials consisting of polymeric and nonpolymeric materials. On the other hand, block polymers[7,8] are examples of microscopically or molecularly hybridized polymeric materials. Typical examples of ABA triblock copolymers are polystyrene-*b*-polyisoprene-*b*-polystyrene (SIS)[9,10] (Figure 1a) and polystyrene-*b*-polybutadiene-*b*-polystyrene (SBS).[11,12] As glassy polystyrene and rubbery polydiene, such as polyisoprene and polybutadiene, are covalently connected in an A−B−A manner, SIS and SBS are used as elastomers with isolated glassy domains of polystyrene at room temperature and rubbery polydiene bridges between the domains. The elastomers exhibit thermoplasticity because the entire material melts at a higher temperature than the T_g of polystyrene; thus, they are called thermoplastic elastomers (TPEs).[13−15] TPEs are useful as processable materials with moderate mechanical properties, and the global market for styrenic block polymer-based TPEs is as large as several billion of dollars.[16] However, the strength of ABA triblock copolymer-based TPEs is not that high and is similar to that of typical filler-unfilled rubber.

There have been several studies on mechanically tough TPEs, such as polyurethane-based TPEs[17−19] with noncovalent bonding groups, especially hydrogen bonding groups; however, ABA triblock copolymer-based TPEs generally do not have noncovalent bonding groups that could enhance their mechanical properties, as they are typically synthesized via

Received: October 8, 2021
Accepted: December 2, 2021
Published: December 20, 2021

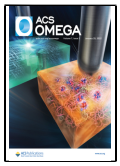

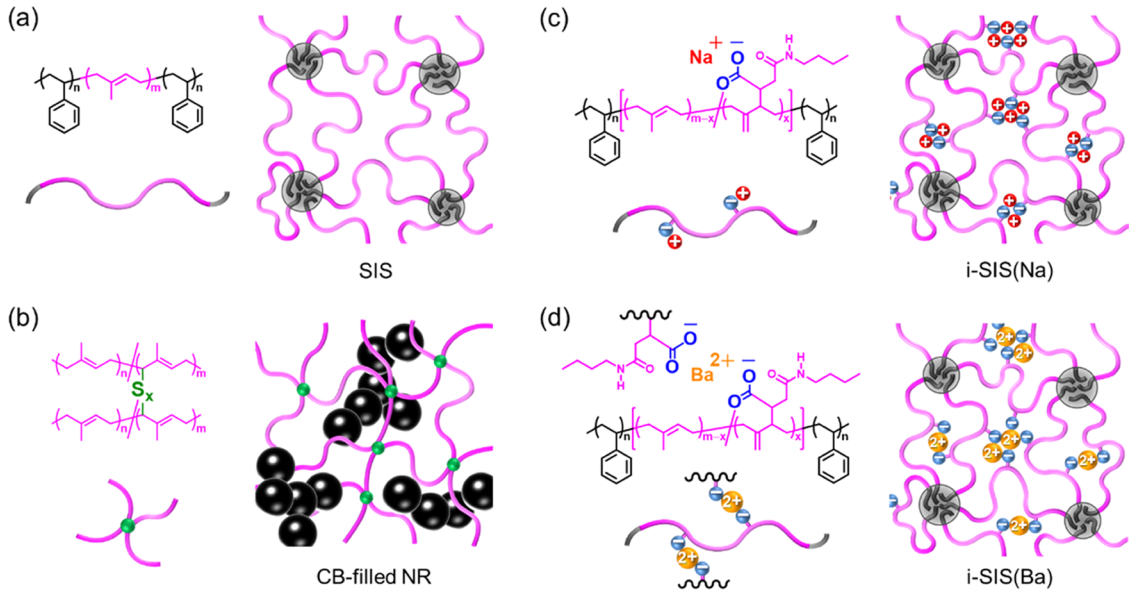

Figure 1. Chemical structures and schematic molecular-level pictures of (a) neat SIS, (b) CB-filled NR,[59] (c) i-SIS(Na), and (d) i-SIS(Ba). The gray spheres depict the isolated glassy polystyrene domains. Blue, red, and orange spheres depict the carboxylate anion, sodium cation, and barium cation, respectively. The black spheres depict particles of carbon black, whereas the small green dots represent a chemical cross-link. See also ref 42.

living anionic polymerization. Recently, the incorporation of noncovalent bonding groups such as hydrogen bonding groups[20−27] or ionic groups[28−34] into the rubber phase matrix of ABA triblock copolymer-based TPEs has been studied in an attempt to increase the TPE strength.[35−42] In 2015, we reported on ABA triblock copolymers with hydrogen bonding groups (e.g., amide groups) in a middle rubber component block[35] and demonstrated that the hydrogen bonds in the rubber matrix contribute to improving the tensile properties of triblock copolymer-based TPEs.[36,38] Other studies also reported hydrogen-bonded ABA triblock copolymer-based TPEs obtained by polymerizing norbornene monomers.[37,39] More recently, we prepared an SIS-based elastomer with ionic functional groups (i-SIS) that exhibited extremely high toughness (W_T = 480 MJ m^{-3}), which is an excellent value compared to previous reports on elastomers, including polyurethane-based TPEs.[42]

Since "tough" means damage-tolerant,[43] i-SIS should exhibit high impact resistance, which is a crucially important mechanical property for practical use, even though i-SIS is a rubber material. However, the impact resistance of almost all advanced elastomeric materials with high performance[18,35−42,44−49] has been hardly evaluated. One of the reasons for this lack of studies is that a relatively large sample is required to carry out impact tests, and a relatively inexpensive and large-scale synthetic scheme has not yet been established for the previously reported advanced elastomeric materials. It should also be emphasized that very few studies on tough advanced elastomers directly compare their mechanical properties with those of other high-strength materials such as FRPs. FRPs cannot be stretched, and their mechanical properties are greatly different from those of largely deformable elastomers, indicating that it is not easy to perform such a comparison; accordingly, previous studies on the tough elastomers merely provide their tensile and other mechanical properties.

In the present study, we evaluated the impact resistance of homogeneous i-SIS(Na) comprising a monovalent sodium cation (Figure 1c) that can be prepared on a scale of several tens of grams by neutralizing the carboxy groups of the precursor of i-SIS, i.e., hydrogen bonding carboxy-functionalized SIS (h-SIS; see our previous report and Figure S1 of the Supporting Information for the synthetic scheme of h-SIS).[42,50,51] Furthermore, we prepared several tens of grams of i-SIS(Ba) (Figure 1d) with a bulky divalent barium cation by neutralizing the carboxy groups of h-SIS with barium ethoxide, and we investigated the effect of the i-SIS cation type on its mechanical properties. Note that hydrogen bonding between the amide groups in i-SIS is much weaker than the short-range ion−ion interactions that arise within ionic multiplets;[52] therefore, the influence of the hydrogen bonds formed between the amide groups in i-SIS on its mechanical properties was assumed to be very small. To evaluate the basic mechanical properties of i-SIS(Na) and i-SIS(Ba), we conducted both tensile tests at different elongation rates and a compression test, and we compared the results with the properties of neat SIS and of carbon black-filled natural rubber (CB-filled NR, Figure 1b).[53,54] CB-filled NR is a typical rubber material and was used as a control sample for neat SIS and i-SIS in terms of elastomeric materials that can be greatly deformed. Finally, drop weight impact tests typically used for evaluation of hard materials, such as FRPs and laminated glasses,[55−58] were performed on i-SIS(Na) and i-SIS(Ba) to investigate their potential as impact-resistant materials and their protection capabilities as a covering material when an impact is directly applied. In addition, the impact resistance of glass fiber-reinforced plastic (GFRP, see also its photo in Figure S2) was used as a high-strength control sample to provide a comparison for the mechanical properties of the tough elastomers.

2. EXPERIMENTAL SECTION

2.1. Materials. Neat SIS (Quintac 3440) was synthesized via sequential living anionic polymerization by Zeon Corporation. The number-average molecular weight and weight fraction of polystyrene were 150 k by GPC and 19

https://doi.org/10.1021/acsomega.1c05609
ACS Omega 2022, 7, 2821−2830

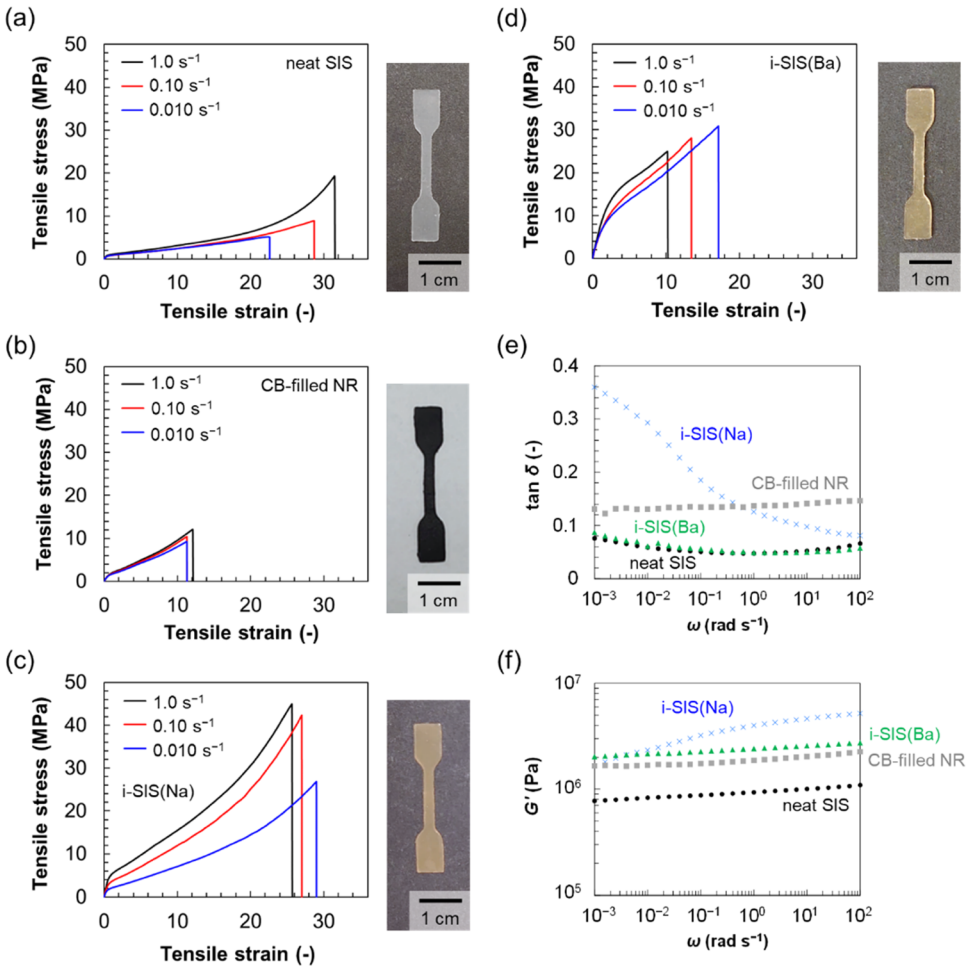

Figure 2. Typical tensile stress−strain curves of (a) neat SIS, (b) CB-filled NR, (c) i-SIS(Na), and (d) i-SIS(Ba) at different elongation rates, where tensile test specimens are also shown. The frequency dependence of (e) tan δ and (f) storage moduli, G', acquired by dynamic mechanical tests for neat SIS, CB-filled NR, i-SIS(Na), and i-SIS(Ba).

wt % by ^{1}H NMR, respectively (see the GPC chromatogram and the ^{1}H NMR spectrum in Figure S3). A 5 mol L^{-1} methanol solution of sodium methoxide and 10% w/v ethanol solution of barium ethoxide were purchased from TCI and Alfa Aesar, respectively. Irgafos 168 and Irganox 565 were purchased from BASF. Epoxy resin-based GFRP with approximately 70 wt % aluminaborosilicate glass (PGE-6635, Ryoden Kasei Co., Ltd.) was used as received, and the weight content of the glass fiber in the GFRP was determined by thermogravimetric analysis (TGA, see Figure S4 in the Supporting Information). The dimension of the GFRP was 100 mm × 50 mm × 4 mm. A 0.5 mm or 4 mm thick CB-filled NR sample with approximately 8 wt % CB (TAKL6503, Tigers Polymer Corporation), which was also determined by TGA, was used for the tensile, compression, and impact tests.

2.2. Synthesis of Block Polymer-Based TPEs with an Ionically Functionalized Rubber Phase. The h-SIS used as the precursor of i-SIS(Na) or i-SIS(Ba) was synthesized as previously reported[42] (see also the chemical structure and the synthetic procedure of h-SIS in Figure S1). The molar content of the carboxyl groups in the polyisoprene block of h-SIS was 5.1 mol %, and all carboxy groups on the h-SIS were neutralized with sodium methoxide to form sodium carboxylate. The specific preparation procedure for i-SIS(Na) was as follows (top of Figure S5): ∼8 g of h-SIS was dissolved in ∼80 g of a mixture of tetrahydrofuran/methanol (9/1 by weight), followed by the addition of ∼0.92 mL of the methanol solution of sodium methoxide to the polymer solution. Note that the molar amount of sodium methoxide (4.6 mmol) in the mixed solution was made equal to the amount of carboxy groups (4.6 mmol) on the h-SIS. Approximately 8 mg of Irgafos 168 and 5.6 mg of Irganox 565 were also added to the solution as antioxidants for the polymer. The neutralized polymer solution was poured into a perfluoroalkoxy alkane (PFA) tray with internal dimensions of 128 mm × 94 mm × 23 mm, and several i-SIS(Na) films with a weight of ∼8 g and a thickness of ∼0.5 mm were finally prepared by a solution-casting method at 45 °C. Several i-SIS(Ba) films with a weight of ∼8 g and a thickness of ∼0.5 mm were also prepared by neutralizing the carboxy groups on h-SIS with ∼5.2 mL of the ethanol solution of barium ethoxide instead of sodium methoxide (bottom of Figure S5). Note that the molar amount of barium ethoxide (2.3 mmol) in the mixed solution was made equal to half the amount of carboxy groups (4.6 mmol) on h-SIS. The small-angle X-ray scattering (SAXS) profile of i-SIS(Ba) was similar to the profile reported previously for i-SIS(Na), indicating that i-SIS(Ba) is probably self-assembled into isolated domain/matrix-based structures like i-SIS(Na). However, the scattering intensity was much lower, probably due to the presence of

https://doi.org/10.1021/acsomega.1c05609
ACS Omega 2022, 7, 2821−2830

Table 1. Tensile Properties of Neat SIS, CB-Filled NR, i-SIS(Na), and i-SIS(Ba) at Different Elongation Rates[a]

sample	$(\dot{\varepsilon}_0)^b$ (s^{-1})	$E_Y{}^c$ (MPa)	$\sigma_{300\%}{}^d$ (MPa)	$\sigma_{max}{}^e$ (MPa)	$\varepsilon_{max}{}^f$ (−)	$W_T{}^g$ (MJ m^{-3})
neat SIS	1.0	2.4 ± 0.07	1.5 ± 0.01	21 ± 1	33 ± 0.9	210 ± 10
	0.10	2.7 ± 0.03	1.1 ± 0.02	9.1 ± 0.2	29 ± 0.2	110 ± 1
	0.010	2.5 ± 0.2	1.3 ± 0.05	6.1 ± 0.5	24 ± 1	77 ± 8
CB-filled NR	1.0	3.7 ± 0.1	3.3 ± 0.02	11 ± 0.7	11 ± 0.5	61 ± 6
	0.10	4.1 ± 0.1	3.0 ± 0.06	8.6 ± 1.0	9.7 ± 0.9	45 ± 8
	0.010	3.7 ± 0.2	2.8 ± 0.05	8.5 ± 0.9	10 ± 0.8	46 ± 7
i-SIS(Na)	1.0	9.1 ± 0.07	5.6 ± 0.2	45 ± 3	25 ± 1	520 ± 50
	0.10	9.8 ± 0.9	5.6 ± 0.2	43 ± 0.9	26 ± 0.7	480 ± 18
	0.010	6.2 ± 0.5	3.2 ± 0.1	23 ± 2	27 ± 2	280 ± 31
i-SIS(Ba)	1.0	7.7 ± 0.5	14 ± 0.9	27 ± 1	11 ± 0.8	190 ± 15
	0.10	8.8 ± 0.3	11 ± 0.6	27 ± 0.7	14 ± 0.4	230 ± 1
	0.010	10 ± 0.7	11 ± 0.2	28 ± 2	17 ± 0.4	280 ± 21

[a]Average value was estimated by measuring three test specimens of the same sample. The standard error of the mean for three measurements is also shown. [b]Initial strain rate. [c]Young's modulus estimated from the slope within a strain range from 0 to 10%. [d]Tensile stress at a strain of 300%. [e]Tensile strength. [f]Elongation at break. [g]Tensile toughness estimated from the inner area of a stress−strain curve.

heavy barium cations (Figure S6 in the Supporting Information).

2.3. Preparation of Test Specimens for Compression and Impact Tests. Test specimens for compression tests were prepared as follows. First, a solution-cast film was cut into pieces of approximately 20 mm × 20 mm × 0.5 mm and stacked. Second, the stacked pieces were pressed for approximately 2 min using a pressing machine under a N_2 atmosphere at 120 °C for neat SIS and i-SIS(Na) and at 150 °C for i-SIS(Ba). The process was repeated three times to prepare a film with a thickness of ∼4 mm. A test specimen was punched out of this film using a round hole punch with a diameter of 8 mm (Figure S7 in the Supporting Information). Note that the prepared specimens can be dissolved in good solvents, such as a tetrahydrofuran/methanol mixture, indicating that the test specimens were not chemically cross-linked during the process of hot-melt pressing.

Test specimens for impact tests were also prepared by punching out the above hot-melt-pressed films. The thickness of the test specimen was 4 mm and the diameter was 25 mm (Figure S7 in the Supporting Information).

2.4. Measurements. To evaluate the tensile properties of elastomers, tensile tests were conducted at ambient temperature with a 10 mm initial specimen distance between jigs using a Shimadzu AGS-X. The elongation rates used were approximately 10, 1.0, or 0.10 mm s^{-1}, and the initial strain rate, $\dot{\varepsilon}_0$, was 1.0, 0.10, or 0.010 s^{-1}, respectively. Test specimens with a thickness of approximately 0.50 mm were prepared by punching out with a die of the standard ISO 37:2017 Type 4 (Figure S7 in the Supporting Information).

Dynamic mechanical shear measurements were performed in an air atmosphere at ambient temperature using an ARES-G2 shear rheometer (TA Instruments) with 8 mm diameter parallel plates within an angular frequency range from 10^2 to 10^{-3} rad s^{-1}.

Compression tests were also carried out using a Shimadzu AGS-X equipped with jigs for compression tests at ambient temperature.[60,61] A compression rate of approximately 0.4 mm s^{-1} was applied with an initial compressive strain rate ($\dot{\varepsilon}_0$) of 0.10 s^{-1}, and the samples were compressed up to ε = 0.975.

Drop weight impact tests were performed in an IM1C-15 (IMATEK) test machine equipped with a rodlike striker with a 16 mm diameter rounded head and a mass (m) of 2.709 kg at 23 °C and 50% RH. The test specimen was fixed on a GFRP support plate with a length of 50 mm, a width of 100 mm, and a thickness of 4 mm (see also Figure S2 in the Supporting Information) using masking tape, and the GFRP support plate was placed on a steel substrate having a length of 150 mm, a width of 100 mm, and a thickness of 10 mm. By dropping a striker from heights in the range from 5 to 87.5 cm, various levels of impact energy were applied to the test specimen. The applied impact energy, E_I, can be estimated from eq 1[62]

$$E_I = mgh - \Delta = \frac{1}{2}mv^2 \quad (1)$$

where g is the gravitational acceleration (9.81 m s^{-2}); h is the height from which the striker is dropped; Δ is the energy loss due to friction or other causes during the weight drop, which can be neglected for simplicity; and v is the velocity of the striker just before it hits the test specimen, which can be measured by the instrument.

3. RESULTS AND DISCUSSION

3.1. Tensile Properties. Uniaxial tensile tests were performed at three different elongation rates to evaluate the rate dependence. Figure 2a−d compares the tensile stress−strain curves of neat SIS, CB-filled NR, i-SIS(Na), and i-SIS(Ba). Table 1 also summarizes the tensile properties, including Young's modulus (E_Y), the stress at a strain of 300% ($\sigma_{300\%}$), the tensile strength (σ_{max}), the elongation at break (ε_{max}), and the tensile toughness (W_T), which can be estimated from the inner area under the stress-strain curve. The E_Y and $\sigma_{300\%}$ of neat SIS were almost independent of the elongation rate and $\dot{\varepsilon}_0$. On the other hand, the σ_{max} and ε_{max} of neat SIS decreased as $\dot{\varepsilon}_0$ decreased; thus, the smaller the $\dot{\varepsilon}_0$, the lower the W_T for the neat SIS (Figure 2a and Table 1). This is probably because the longer duration of the elongation due to the lower elongation rate may have caused a gradual pull-out of polystyrene chains from the glassy isolated domain, leading to the failure of the neat SIS at this lower elongation. In contrast to the tensile properties of neat SIS, those of CB-filled NR made of a chemically cross-linked polymer network were almost independent of the elongation rate, with E_Y of ∼4 MPa, $\sigma_{300\%}$ ∼3 MPa, σ_{max} ∼9 MPa, ε_{max} ∼10, and W_T ∼50 MJ m^{-3} (Figure 2b and Table 1). As the fracture of CB-filled NR was attributed to the breaking of covalent bonds at the covalent-bonded cross-links or the polymer network, the tensile properties of CB-filled NR did not strongly depend on the

https://doi.org/10.1021/acsomega.1c05609
ACS Omega 2022, 7, 2821−2830

elongation period associated with the elongation rate; therefore, the tensile behavior of neat SIS fairly differed from that of CB-filled NR due to the difference in the fracture mechanism.

On the other hand, as $\dot{\varepsilon}_0$ decreased, the $\sigma_{300\%}$, σ_{max}, and W_T of i-SIS(Na) decreased but ε_{max} slightly increased (Figure 2c and Table 1). Comparing tensile properties, i-SIS(Na) exhibited much higher E_Y, $\sigma_{300\%}$, σ_{max}, and W_T than neat SIS, and i-SIS(Na) also kept a relatively high ε_{max} (>25) without being strongly dependent on $\dot{\varepsilon}_0$. In particular, i-SIS(Na) attained a W_T of 520 MJ m^{-3} at an $\dot{\varepsilon}_0$ of 1.0 s^{-1}, which is an excellent value in terms of toughness.[42] The exceptional tensile properties of i-SIS(Na) arise probably because the ionic multiplets[63,64] formed by aggregation of multiple sodium cations and carboxylate anions that serve as reversible and dynamic cross-links induce a high tensile stress when the sample is deformed, whereas fracturing at a small elongation is suppressed by hindering the pull-out of polystyrene chains from the glassy domains. This contrasts with the case of neat SIS due to dissipation of the local high stress by disassembly of the ionic multiplets. According to dynamic frequency sweeps within a wide frequency range, the tan δ of neat SIS and CB-filled NR were 0.076 and 0.13 at very low frequencies of ~10^{-3} rad s^{-1}, respectively, whereas i-SIS(Na) had a relatively large tan δ value (~0.3) at the same frequencies (Figure 2e), suggesting that i-SIS(Na) has a slow relaxation mode originating from the reversible recombination of ionic multiplets by disassembly/reassembly. Note that the storage modulus (G') of i-SIS(Na) was higher than that of neat SIS within the adopted frequency range (Figure 2f), supporting the higher E_Y of i-SIS(Na) compared to neat SIS as revealed by the tensile tests (see also Figure S8 for the loss moduli).

The E_Y was about the same for both i-SIS(Ba) with the divalent cation and i-SIS(Na), but the $\sigma_{300\%}$ was more than twice as high for i-SIS(Ba) than i-SIS(Na) (Figure 2d and Table 1). On the other hand, the ε_{max} of i-SIS(Ba) ranged from 10 to 20, which was about the same as or higher than that of CB-filled NR but much lower than that of i-SIS(Na). As $\dot{\varepsilon}_0$ decreased, the ε_{max} of i-SIS(Ba) increased, which was the same trend observed for i-SIS(Na). However, the ε_{max} of i-SIS(Ba) was 17 even when $\dot{\varepsilon}_0$ was 0.01 s^{-1}, and the fracture of i-SIS(Ba) occurred at a relatively low elongation compared to that of i-SIS(Na) (Figure 2c and Table 1). Because the divalent cation in i-SIS(Ba) is bulky and must be paired with two carboxylate anions to satisfy electrical neutrality at the microscale, the recombination rate for the disassembly/reassembly of the ionic multiplets of i-SIS(Ba) is much slower than that for i-SIS(Na), leading to a lower ε_{max} for i-SIS(Ba) compared to i-SIS(Na). Interestingly, even though the ionic multiplets in i-SIS(Ba) should have a finite lifetime for disassembly, its tan δ obtained by linear dynamic viscoelasticity measurements did not show any distinct peak or increase within the measurement frequency range (10^2–10^{-3} rad s^{-1}) (Figure 2e), implying that the relaxation would be observed at frequencies <10^{-3} rad s^{-1}. Note that smooth master curves cannot be created, even when attempting to superpose the frequency sweep data at several temperatures.[65−67] This is because i-SIS has at least two independent relaxation modes, such as one originating from the equilibration of deformed polymer chains and one associated with reversible recombination of ionic multiplets by disassembly/reassembly (see also the temperature sweep for i-SIS(Ba) in Figure S9 of the Supporting Information).

3.2. Compressive Properties. Rubber materials in use are not always elongated but are often compressed. Because compression occurs first when a large impact is applied to the material, it is important to know the compression properties of the material before evaluating its impact properties. In this study, the compression properties of the elastomers were evaluated using a specimen with a diameter of 8 mm and a thickness of 4 mm. The compression rate was 0.4 mm s^{-1} and $\dot{\varepsilon}_0$ was 0.10 s^{-1}. Figure 3 compares the compressive stress–strain curves of neat SIS, CB-filled NR, i-SIS(Na), and i-SIS(Ba). Table 2 summarizes the compressive modulus estimated from the slope within a strain range of 0–5% (E_C), the compressive stress at a compressive strain of 97.5% ($\sigma_{C,97.5\%}$), and the compressive toughness ($W_{C,97.5\%}$) that can be estimated from the inner area under the stress–strain curve up to a strain of 97.5%. No fracture was observed in any of the specimens, even with compression up to ε = 0.975, and the specimens immediately returned to almost the original dimension when the compressive stress was removed. As shown in Figure 3 and Table 2, neat SIS exhibited an E_C of 2.9 MPa, $\sigma_{C,97.5\%}$ of 85 MPa, and $W_{C,97.5\%}$ of 12 MJ m^{-3}. In contrast, NR with carbon black that is a high-strength filler (E ~ 10 GPa[68]) exhibited a higher E_C of 7.7 MPa and $\sigma_{C,97.5\%}$ of 160 MPa probably due to the reinforcing effect of the filler; thus, CB-filled NR was deformed less by the same degree of compressive stress than neat SIS. Although lacking a filler and being thermoplastic, i-SIS(Na) exhibited much higher compression properties than neat SIS and the same degree of compression resistance as CB-filled NR (E_C = 8.5 MPa, $\sigma_{C,97.5\%}$ = 160 MPa, $W_{C,97.5\%}$ = 29 MJ m^{-3}). More remarkably, i-SIS(Ba) exhibited even higher compression properties than i-SIS(Na) and CB-filled NR (E_C = 8.3 MPa, $\sigma_{C,97.5\%}$ = 190 MPa, and $W_{C,97.5\%}$ = 38 MJ m^{-3}), which indicated that i-SIS(Ba) is

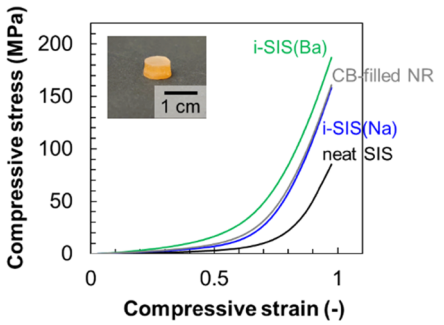

Figure 3. Compressive stress–strain curves of neat SIS, CB-filled NR, i-SIS(Na), and i-SIS(Ba) at $\dot{\varepsilon}_0$ = 0.10 s^{-1}. Inset: photograph of a typical i-SIS(Na) test specimen for compression.

Table 2. Compressive Properties of Neat SIS, CB-filled NR, i-SIS(Na), and i-SIS(Ba) at $\dot{\varepsilon}_0$ = 0.10 s^{-1}

sample	E_C[a] (MPa)	$\sigma_{C,97.5\%}$[b] (MPa)	$W_{C,97.5\%}$[c] (MJ m^{-3})
neat SIS	2.9	85	12
CB-filled NR	7.7	160	29
i-SIS(Na)	8.5	160	27
i-SIS(Ba)	8.3	190	38

[a]Compressive modulus estimated from the slope within a strain range of 0–5%. [b]Compressive stress at a compressive strain of 97.5%. [c]Compressive toughness estimated from the inner area of a stress–strain curve up to a compressive strain of 97.5%.

https://doi.org/10.1021/acsomega.1c05609
ACS Omega 2022, 7, 2821−2830

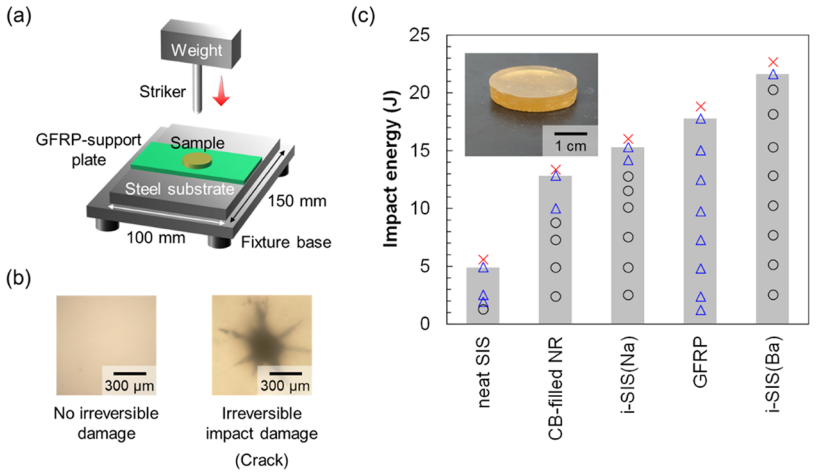

Figure 4. Evaluation of impact properties by drop weight impact tests. (a) Schematic of the experimental setup for drop weight impact tests. (b) Optical microscopy images of the test specimens after the drop weight impact tests for neat SIS. The left and right images show the neat SIS specimen after the striker is dropped from heights of 5.0 and 7.5 cm, respectively. (c) Relationships between the applied E_I and impact resistance of neat SIS, CB-filled NR, i-SIS(Na), epoxy resin-based GFRP, and i-SIS(Ba). Inset: photograph of a typical test specimen. Open black circles represent E_I applied without any irreversible damage, such as cracks or dents, on both test specimens and the GFRP support plate. Open blue triangles represent E_I applied when irreversible impact damage was caused to the specimen but no damage occurred to the GFRP support plate. Red crosses represent E_I applied when irreversible damage occurred to both the test specimen and the GFRP support plate. Bars represent $E_{I,max,protect}$, which is the maximum E_I that can be applied to test specimens when any irreversible damage to a GFRP support plate covered by the test specimens was not caused by the drop weight impact. Note that irreversible damage to a GFRP plate can easily be caused by a small applied E_I of ∼1.2 J (h = 5.0 cm).

an extremely high-strength rubber material with respect to compression. Note that when a stress of 190 MPa was applied to the specimen of i-SIS(Ba) with the above-mentioned dimensions, the applied force was approximately 9.5 kN (∼970 kgf). The high compression resistance of i-SIS(Ba) was attributed to the presence of ionic multiplets comprising bulky divalent cations that should cause strong ionic interactions among ions.

3.3. Impact-Resistant Properties. As i-SIS(Na) and i-SIS(Ba) have high toughness in terms of tensile elongation and compression, they resist impacts and are not easily damaged, even by strong and local compression resulting from a drop weight impact. Therefore, drop weight impact tests that require a large amount of sample materials were conducted to directly observe their impact resistance. A striker was dropped from height h to apply a strong compressive impact to a test specimen. The specimen had a thickness of approximately 4 mm and was placed on a 4 mm thick GFRP support plate that could be damaged easily with impact (Figure 4). The experimental impact energy (E_I) is the maximum energy value in the energy−time curve, which is a plot of the energy applied to the test specimen against time after the striker hits the test specimen (Figure S10 in the Supporting Information).

Figure 4b compares optical microscopy images of the test specimen of neat SIS after the drop weight impact tests. The left image is the test specimen after applying E_I = 1.23 J (h = 5.0 cm), whereas the right image is after applying E_I = 1.89 J (h = 7.5 cm) (see also Table S1 in the Supporting Information). Images of other specimens are shown in Figure S11. Obviously, no irreversible impact damage, such as cracks, was seen with the former, whereas a radical crack is observed for the latter. The crack could not be self-repaired, even if left for one week at room temperature. Therefore, the irreversible damage resistance of elastomers can be evaluated by determining $E_{I,min,damage}$, i.e., the minimum E_I when damage is caused to the test specimen.[69,70] Figure 4c compares E_I applied to neat SIS, CB-filled NR, i-SIS(Na), GFRP, and i-SIS(Ba), where open black circles represent E_I applied without any irreversible damage, such as cracks or dents, on both test specimens and the GFRP support plate. Open blue triangles represent E_I applied when irreversible impact damage was caused to the specimen but there was no damage of the GFRP support plate. $E_{I,min,damage}$ expresses the level of damage resistance of these materials, and the mechanical properties of GFRP are summarized in Tables S1 and S2 in the Supporting Information, respectively (see also tensile stress−strain curves of GFRP in Figure S12). For CB-filled NR, irreversible damage was not observed even when the applied E_I was 8.74 J, which is approximately five times higher than the 1.87 J that caused a radical crack on neat SIS (see also Table S1 in the Supporting Information). Crack initiation for CB-filled NR was finally observed at E_I = 9.99 J. Therefore, CB-filled NR exhibits higher damage resistance than neat SIS probably due to the incorporation of CB as a reinforced filler in the rubber phase.

Drop weight impact tests were also performed for i-SIS(Na). Irreversible damage was not observed for i-SIS(Na), even when applying E_I = 12.8 J, which is approximately seven times higher than the 1.87 J that caused a radical crack on neat SIS. Crack initiation for i-SIS(Na) was finally observed at E_I = 14.2 J; therefore, i-SIS(Na) exhibits higher $E_{I,min,damage}$ than conventional SIS and CB-filled NR. We attribute the excellent damage resistance of i-SIS(Na) to the effective stress/energy-dissipation mechanism, i.e., the disassembly of strongly associated ionic multiplets into multiple ion pairs.[71,72] This mechanism probably prevents the easy material fracture typically caused by the breaking of covalent bonds in polymer chains or the polystyrene hard domains. The damage resistance of i-SIS(Ba) was also examined by the same tests. As evident from Figure 4c and Table S1, i-SIS(Ba) with a divalent cation exhibited even greater damage resistance ($E_{I,min,damage}$ = 21.6 J) than i-SIS(Na) ($E_{I,min,damage}$ =14.2 J). This high and excellent

https://doi.org/10.1021/acsomega.1c05609
ACS Omega 2022, 7, 2821−2830

impact damage resistance is probably due to the presence of the divalent ions, which cause a stronger association among ionic multiplets in the soft rubber phase. Therefore, i-SIS(Ba) is a rubber material that is highly tolerant of not only simple compression but also local compression with drop weight impact.

For structure material applications, it is important for the material to protect other materials that it covers, even when the covering material is completely fractured or compressed by the impact. This capability can be referred to as the impact resistance needed to protect covered materials from damage.[73,74] To evaluate such an impact resistance, a higher E_I was applied to the test specimen than the $E_{I,min,damage}$ that causes irreversible damage to the test specimen. The red crosses in Figure 4c represent E_I applied when irreversible damage occurred to both the test specimen of covering materials and the GFRP support plate of a covered material. Table 3 summarizes $E_{I,max,protect}$, i.e., the maximum E_I that can be applied to test specimens on the easily damaged GFRP support plate of a covered material without irreversible damage to the GFRP support plate. As evident in Table 3 and Figure 4c, the $E_{I,max,protect}$, which expresses the level of impact resistance, was higher for typical commercially available vulcanized rubber such as CB-filled NR (12.8 J) than it was for neat SIS (4.90 J).

Table 3. Impact Resistance of Covering Materials that Protect Covered Materials from Being Damaged, as Estimated by Drop Weight Impact Tests

sample	$E_{I,max,protect}$ [a] (J)	h [b] (cm)
neat SIS	4.90	20.0
CB-filled NR	12.8	50.0
i-SIS(Na)	15.3	60.0
GFRP	17.8	70.0
i-SIS(Ba)	21.6	85.0

[a]Maximum impact energy that can be applied such that irreversible impact damage occurs only to the specimen and not to the GFRP support plate. The tests were performed using a rodlike striker with a 16 mm rounded head (mass 2.709 kg) at 23 °C and 50% RH. [b]Maximum height position of the striker for a drop weight impact test such that irreversible impact damage occurs only to the specimen and not to the GFRP support plate.

Concerning the drop weight impact tests of i-SIS(Na) on the GFRP support plate, irreversible damage of the covered GFRP support plate was not observed up to an E_I of 15.3 J, indicating a higher impact resistance than that of CB-filled NR, even though i-SIS(Na) lacks a filler, is not chemically cross-linked, and can be reprocessed. Notably, damage to the GFRP support plate was not observed up to an E_I of 21.6 J when i-SIS(Ba) with divalent barium cations was used as a covering material for the GFRP support plate. It should be emphasized that irreversible damage occurred to a 4 mm thick GFRP support plate covered by another 4 mm thick GFRP plate (Figure 4c) when applying an E_I of 18.8 J, suggesting that i-SIS(Ba) with the same thickness exhibited higher $E_{I,max,protect}$ (impact resistance) than GFRP, even though GFRP is a so-called high-strength material that is used, for example, as automobile bumpers and interior parts. The excellent impact resistance of i-SIS(Ba) probably originates from both the softness of the rubber phase and the presence of rigid ionic multiplets formed by divalent barium cations with the slow relaxation mode that is supported by the frequency sweep of i-SIS(Ba) in Figure 2e. Such divalent cations probably cause a stronger association and promote physical cross-linking of the rubber phase. Considering the above results, it could be possible to prepare excellent impact-resistant materials as products by laminating i-SIS(Ba) and GFRP.[56] In total, the block polymer-based TPEs with an ionically functionalized rubber phase, especially those using divalent ions, were highly impact resistant, even though they did not incorporate inorganic fillers and were not chemically cross-linked.

4. CONCLUSIONS

In this study, several tens of grams of i-SIS(Na) or i-SIS(Ba) were prepared by neutralizing the carboxy groups on h-SIS with metal alkoxides. Their impact resistance was also evaluated quantitatively. Tensile tests revealed that i-SIS(Na) had a relatively high ε_{max} (>25) at any $\dot{\varepsilon}_0$. In addition, i-SIS(Na) attained the excellent value of W_T (520 MJ m^{-3}) at $\dot{\varepsilon}_0$ = 1.0 s^{-1}, which is much higher than that of neat SIS. Although i-SIS(Ba) exhibited a lower W_T (280 MJ m^{-3}) than i-SIS(Na) at $\dot{\varepsilon}_0$ = 0.010 s^{-1}, the tensile toughness of i-SIS(Ba) was still higher than that of neat SIS. This high W_T of i-SIS(Na) and i-SIS(Ba) probably originates from the presence of ionic multiplets consisting of the metal cations and the carboxylate anion. These serve as reversible and dynamic cross-links in the ionically functionalized rubber phase and disperse local high stress, with the valence of metal cations also affecting the tensile properties. In compression tests, stresses of 85, 160, and 160 MPa were generated when a compressive strain of 97.5% was applied to neat SIS, i-SIS(Na), and CB-filled NR, respectively, indicating that the compressive resistance of i-SIS(Na) was much higher than that of neat SIS and almost the same as conventional CB-filled rubber, even though i-SIS(Na) showed thermoplasticity. Moreover, i-SIS(Ba) attained a $\sigma_{C,97.5\%}$ of 190 MPa, higher than that for i-SIS(Na), indicating that i-SIS(Ba) is a high-strength material not only for tensile elongation but also for compression.

Finally, the impact resistances of i-SIS(Na) and i-SIS(Ba) were evaluated by drop weight impact tests and directly compared to that of a high-strength GFRP. To perform quantitative evaluation and direct comparison of the impact resistances of such different materials, this study used the original experimental setup for the drop weight impact tests and defined two parameters ($E_{I,min,damage}$ and $E_{I,max,protect}$) to evaluate the impact resistance. $E_{I,max,protect}$ of i-SIS(Na) was 15.3 J; i.e., irreversible damage on the material covered by i-SIS(Na) was not observed up to E_I = 15.3 J. Therefore, even without a filler, i-SIS(Na) was superior to neat SIS and CB-filled NR in terms of not only the tensile properties but also the impact resistance. Remarkably, when using i-SIS(Ba) as a covering material, the $E_{I,max,protect}$ that can be applied without irreversible damage to the covered materials is 21.6 J, which is higher than the $E_{I,max,protect}$ (17.8 J) when GFRP is used as a covering material; thus, i-SIS(Ba) exhibits excellent impact resistance for protection superior to GFRP as a typical high-strength material. All of these findings are attributed to not only the softness of the rubber phase but also the hardness of the dynamic and reversible ionic multiplets formed by cations and anions, especially for the divalent bulky cations and anions that cause a stronger association. Since the triblock copolymer-based TPEs with the ionically functionalized rubber phase used in this study can be synthesized industrially on a large scale, they have great market potential as next-generation elastomeric

https://doi.org/10.1021/acsomega.1c05609
ACS Omega 2022, 7, 2821−2830

materials for practical use. Thus, they can be applied to not only interior/exterior parts but also to body parts or outer panels of automobiles, trains, or other vehicles that probably require elastomeric materials with excellent mechanical properties as well as processability. In the future, we will report on the influence of the ion concentration on the mechanical properties of i-SIS. Furthermore, we will also investigate the mechanical properties of i-SIS without hydrogen bonding amide groups to reveal the influence of the hydrogen bonds formed in the i-SIS of this study.

■ ASSOCIATED CONTENT

Supporting Information

The Supporting Information is available free of charge at https://pubs.acs.org/doi/10.1021/acsomega.1c05609.

Synthesis of h-SIS; photo of the GFRP plate; GPC chromatogram and ^{1}H NMR spectrum of neat SIS; weight content of the glass fiber in the GFRP; synthetic scheme of i-SIS(Na) and i-SIS(Ba); SAXS measurement; specimen shape and dimension for various measurements; frequency dependence of storage moduli, G', and loss moduli, G''; temperature dependence of G', G'', and $\tan\delta$; energy−time curves acquired by drop weight impact tests; optical microscopy images of the test specimens after the drop weight impact tests; mechanical properties of the GFRP (Figures S1−S12 and Tables S1−S2) (PDF)

■ AUTHOR INFORMATION

Corresponding Author

Atsushi Noro − *Department of Molecular & Macromolecular Chemistry, Graduate School of Engineering, Nagoya University, Nagoya 464-8603, Japan; Institute of Materials Innovation, Institutes of Innovation for Future Society, Nagoya University, Nagoya 464-8601, Japan;* orcid.org/0000-0002-3336-763X; Email: noro@nagoya-u.jp

Authors

Takato Kajita − *Department of Molecular & Macromolecular Chemistry, Graduate School of Engineering, Nagoya University, Nagoya 464-8603, Japan*

Ryoji Oda − *Zeon Corporation, Tokyo 100-8246, Japan;* orcid.org/0000-0002-0108-1442

Sadaharu Hashimoto − *Zeon Corporation, Tokyo 100-8246, Japan*

Complete contact information is available at: https://pubs.acs.org/10.1021/acsomega.1c05609

Author Contributions

A.N. conceived the original idea and designed the study with all other authors. T.K. carried out most of the experiments. A.N. and T.K. analyzed the data. A.N. and T.K. co-wrote the paper with input from all authors.

Notes

The authors declare the following competing financial interest(s): 1. Patent applicant: Nagoya University; Name of inventors: Atsushi Noro, Mikihiro Hayashi, Ryusuke Hiramatsu, Yushu Matsushita; Application number: JP2014-227272; Title: Non-covalent bonded elastomer. 2. Patent applicant: Nagoya University; Name of inventors: Atsushi Noro, Maho Ohno; Application number: PCT/JP2016/063152; Title: Non-covalent bonding soft elastomer and production process therefor. 3. Patent applicant: Zeon Corporation, Nagoya University; Name of inventors: Kosuke Isobe, Sadaharu Hashimoto, Atsushi Nozawa, Ryoji Kameyama, Atsushi Noro, Takato Kajita, Yushu Matsushita; Application number: PCT/JP2018/017439; Title: Block copolymer composition obtained by modification treatment, method for producing same, modified block copolymer composition used for same, and method for producing said modified block copolymer composition. 4. Patent applicant: Zeon Corporation, Nagoya University; Name of inventors: Kosuke Isobe, Sadaharu Hashimoto, Atsushi Nozawa, Atsushi Noro, Takato Kajita, Yushu Matsushita; Application number: PCT/JP2018/031200; Title: Multi-block copolymer composition obtained by modification treatment, and film. 5. Patent applicant: Zeon Corporation, Nagoya University; Name of inventors: Kosuke Isobe, Sadaharu Hashimoto, Atsushi Noro, Takato Kajita, Haruka Tanaka, Yushu Matsushita; Application number: PCT/JP2019/017675; Title: Block copolymer composition having ionic group and film.

■ ACKNOWLEDGMENTS

The authors thank Prof. Yushu Matsushita at Toyota Physical and Chemical Research Institute for kind advice on block polymer studies, Prof. Kenji Urayama at Kyoto Institute of Technology for his kind suggestions on the tensile tests, and Prof. Yohei Miwa at Gifu University for his kind advice on ionically functionalized rubber materials. The authors also thank Kondo at Industrial Technology Center of Fukui Prefecture, Japan, for his kind help with the drop weight impact tests; Futamura at Nagoya Municipal Industrial Research Institute, Japan, for his assistance in mechanical property measurements; Higuchi at High Voltage Electron Microscope Laboratory in Nagoya University for his support in the observation of samples damaged by impact; and Hikage at the High Intensity X-ray Diffraction Laboratory at Nagoya University for his assistance in SAXS measurements. This work was supported through the Collaborative Research Program of the Institute for Chemical Research, Kyoto University (grant #2019-58 and #2020-56). This work was also partially supported through KAKENHI Grants 15K13785 (A.N.), 21K05197 (A.N.), and 20J11033 (T.K.) from JSPS, Japan.

■ REFERENCES

(1) Brazel, C. S.; Rosen, S. L. *Fundamental Principles of Polymeric Materials*; 3rd ed.; Wiley: New York, 2012.

(2) Chawla, K. K. *Composite Materials*, 3rd ed.; Springer: New York, 2012.

(3) Hsissou, R.; Seghiri, R.; Benzekri, Z.; Hilali, M.; Rafik, M.; Elharfi, A. Polymer Composite Materials: A Comprehensive Review. *Compos. Struct.* **2021**, *262*, No. 113640.

(4) Sathishkumar, T. P.; Satheeshkumar, S.; Naveen, J. Glass Fiber-Reinforced Polymer Composites − a Review. *J. Reinf. Plast. Compos.* **2014**, *33*, 1258−1275.

(5) Yao, S.-S.; Jin, F.-L.; Rhee, K. Y.; Hui, D.; Park, S.-J. Recent Advances in Carbon-Fiber-Reinforced Thermoplastic Composites: A Review. *Composites, Part B* **2018**, *142*, 241−250.

(6) Cantwell, W. J.; Morton, J. The Impact Resistance of Composite Materials — a Review. *Composites* **1991**, *22*, 347−362.

(7) Matsen, M. W.; Bates, F. S. Unifying Weak- and Strong-Segregation Block Copolymer Theories. *Macromolecules* **1996**, *29*, 1091−1098.

(8) Lodge, T. P. Block Copolymers: Past Successes and Future Challenges. *Macromol. Chem. Phys.* **2003**, *204*, 265−273.

(9) Uchida, T.; Soen, T.; Inoue, T.; Kawai, H. Domain Structure and Bulk Properties of Solvent-Cast Films of A−B−A Block Copolymers of Styrene-Isoprene-Styrene. *J. Polym. Sci., Part A-2* **1972**, *10*, 101−121.
(10) Watanabe, H. Slow Dielectric Relaxation of a Styrene-Isoprene-Styrene Triblock Copolymer with Dipole Inversion in the Middle Block: A Challenge to a Loop/Bridge Problem. *Macromolecules* **1995**, *28*, 5006−5011.
(11) Matsuo, M.; Ueno, T.; Horino, H.; Chujyo, S.; Asai, H. Fine Structures and Physical Properties of Styrene-Butadiene Block Copolymers. *Polymer* **1968**, *9*, 425−436.
(12) Widin, J. M.; Schmitt, A. K.; Schmitt, A. L.; Im, K.; Mahanthappa, M. K. Unexpected Consequences of Block Polydispersity on the Self-Assembly of ABA Triblock Copolymers. *J. Am. Chem. Soc.* **2012**, *134*, 3834−3844.
(13) Holden, G.; Bishop, E. T.; Legge, N. R. Thermoplastic Elastomers. *J. Polym. Sci., Part C: Polym. Symp.* **1969**, *26*, 37−57.
(14) Holden, G.; Legge, N. R.; Quirk, R.; Schroeder, H. E. *Thermoplastic Elastomers*, 2nd ed.; Hanser Publications: Cincinnati, 1996.
(15) Wang, W.; Lu, W.; Goodwin, A.; Wang, H.; Yin, P.; Kang, N.-G.; Hong, K.; Mays, J. W. Recent Advances in Thermoplastic Elastomers from Living Polymerizations: Macromolecular Architectures and Supramolecular Chemistry. *Prog. Polym. Sci.* **2019**, *95*, 1−31.
(16) *Thermoplastic Elastomer Market Size, Share & Trends Analysis Report by Product, by Application, and Segment Forecasts, 2016−2022*; Grand View Research: San Francisco, 2016.
(17) Hepburn, C. *Polyurethane Elastomers*; Elsevier Applied Science: London, 1992.
(18) Fernández-d'Arlas, B.; Ramos, J. A.; Saralegi, A.; Corcuera, M.; Mondragon, I.; Eceiza, A. Molecular Engineering of Elastic and Strong Supertough Polyurethanes. *Macromolecules* **2012**, *45*, 3436−3443.
(19) Wang, D.; Xu, J.; Chen, J.; Hu, P.; Wang, Y.; Jiang, W.; Fu, J. Transparent, Mechanically Strong, Extremely Tough, Self-Recoverable, Healable Supramolecular Elastomers Facilely Fabricated via Dynamic Hard Domains Design for Multifunctional Applications. *Adv. Funct. Mater.* **2020**, *30*, No. 1907109.
(20) Sijbesma, R. P.; Beijer, F. H.; Brunsveld, L.; Folmer, B. J. B.; Hirschberg, J. H. K. K.; Lange, R. F. M.; Lowe, J. K. L.; Meijer, E. W. Reversible Polymers Formed from Self-Complementary Monomers Using Quadruple Hydrogen Bonding. *Science* **1997**, *278*, 1601−1604.
(21) Chino, K.; Ashiura, M. Themoreversible Cross-Linking Rubber Using Supramolecular Hydrogen-Bonding Networks. *Macromolecules* **2001**, *34*, 9201−9204.
(22) Mather, B. D.; Baker, M. B.; Beyer, F. L.; Berg, M. A. G.; Green, M. D.; Long, T. E. Supramolecular Triblock Copolymers Containing Complementary Nucleobase Molecular Recognition. *Macromolecules* **2007**, *40*, 6834−6845.
(23) Cordier, P.; Tournilhac, F.; Soulié-Ziakovic, C.; Leibler, L. Self-Healing and Thermoreversible Rubber from Supramolecular Assembly. *Nature* **2008**, *451*, 977−980.
(24) Noro, A.; Matsushita, Y.; Lodge, T. P. Thermoreversible Supramacromolecular Ion Gels via Hydrogen Bonding. *Macromolecules* **2008**, *41*, 5839−5844.
(25) Feldman, K. E.; Kade, M. J.; Meijer, E. W.; Hawker, C. J.; Kramer, E. J. Model Transient Networks from Strongly Hydrogen-Bonded Polymers. *Macromolecules* **2009**, *42*, 9072−9081.
(26) Pitet, L. M.; van Loon, A. H. M.; Kramer, E. J.; Hawker, C. J.; Meijer, E. W. Nanostructured Supramolecular Block Copolymers Based on Polydimethylsiloxane and Polylactide. *ACS Macro Lett.* **2013**, *2*, 1006−1010.
(27) Zhang, H. J.; Sun, T. L.; Zhang, A. K.; Ikura, Y.; Nakajima, T.; Nonoyama, T.; Kurokawa, T.; Ito, O.; Ishitobi, H.; Gong, J. P. Tough Physical Double-Network Hydrogels Based on Amphiphilic Triblock Copolymers. *Adv. Mater.* **2016**, *28*, 4884−4890.
(28) Weiss, R. A.; Sen, A.; Willis, C. L.; Pottick, L. A. Block Copolymer Ionomers: 1. Synthesis and Physical Properties of Sulphonated Poly(Styrene-Ethylene/Butylene-Styrene). *Polymer* **1991**, *32*, 1867−1874.
(29) Hunt, J. N.; Feldman, K. E.; Lynd, N. A.; Deek, J.; Campos, L. M.; Spruell, J. M.; Hernandez, B. M.; Kramer, E. J.; Hawker, C. J. Tunable, High Modulus Hydrogels Driven by Ionic Coacervation. *Adv. Mater.* **2011**, *23*, 2327−2331.
(30) Sun, T. L.; Kurokawa, T.; Kuroda, S.; Ihsan, A. Bin.; Akasaki, T.; Sato, K.; Haque, M. A.; Nakajima, T.; Gong, J. P. Physical Hydrogels Composed of Polyampholytes Demonstrate High Toughness and Viscoelasticity. *Nat. Mater.* **2013**, *12*, 932−937.
(31) Mayumi, K.; Marcellan, A.; Ducouret, G.; Creton, C.; Narita, T. Stress−Strain Relationship of Highly Stretchable Dual Cross-Link Gels: Separability of Strain and Time Effect. *ACS Macro Lett.* **2013**, *2*, 1065−1068.
(32) Mohanty, A. D.; Ryu, C. Y.; Kim, Y. S.; Bae, C. Stable Elastomeric Anion Exchange Membranes Based on Quaternary Ammonium-Tethered Polystyrene-*b*-poly(ethylene-*co*-butylene)-*b*-polystyrene Triblock Copolymers. *Macromolecules* **2015**, *48*, 7085−7095.
(33) Miwa, Y.; Taira, K.; Kurachi, J.; Udagawa, T.; Kutsumizu, S. A gas-plastic elastomer that quickly self-heals damage with the aid of CO_2 gas. *Nat. Commun.* **2019**, *10*, No. 1828.
(34) Kajita, T.; Tanaka, H.; Noro, A.; Matsushita, Y.; Nakamura, N. Acidic liquid-swollen polymer membranes exhibiting anhydrous proton conductivity higher than 100 mS cm^{-1} at around 100 °C. *J. Mater. Chem. A* **2019**, *7*, 15585−15592.
(35) Hayashi, M.; Matsushima, S.; Noro, A.; Matsushita, Y. Mechanical Property Enhancement of ABA Block Copolymer-Based Elastomers by Incorporating Transient Cross-Links into Soft Middle Block. *Macromolecules* **2015**, *48*, 421−431.
(36) Hayashi, M.; Noro, A.; Matsushita, Y. Highly Extensible Supramolecular Elastomers with Large Stress Generation Capability Originating from Multiple Hydrogen Bonds on the Long Soft Network Strands. *Macromol. Rapid Commun.* **2016**, *37*, 678−684.
(37) Yang, J.-X.; Long, Y.-Y.; Pan, L.; Men, Y.-F.; Li, Y.-S. Spontaneously Healable Thermoplastic Elastomers Achieved through One-Pot Living Ring-Opening Metathesis Copolymerization of Well-Designed Bulky Monomers. *ACS Appl. Mater. Interfaces* **2016**, *8*, 12445−12455.
(38) Kajita, T.; Noro, A.; Matsushita, Y. Design and properties of supramolecular elastomers. *Polymer* **2017**, *128*, 297−310.
(39) Yoshida, S.; Ejima, H.; Yoshie, N. Tough Elastomers with Superior Self-Recoverability Induced by Bioinspired Multiphase Design. *Adv. Funct. Mater.* **2017**, *27*, No. 1701670.
(40) Ding, W.; Robertson, M. L. Sustainable Thermoplastic Elastomers with a Transient Network. *Eur. Polym. J.* **2019**, *113*, 411−423.
(41) Yan, M.; Cao, L.; Xu, C.; Chen, Y. Fabrication of "Zn^{2+} Salt-Bondings" Cross-Linked SBS-*g*-COOH/ZnO Composites: Thiol−Ene Reaction Modification of SBS, Structure, High Modulus, and Shape Memory Properties. *Macromolecules* **2019**, *52*, 4329−4340.
(42) Kajita, T.; Tanaka, H.; Noro, A.; Matsushita, Y.; Nozawa, A.; Isobe, K.; Oda, R.; Hashimoto, S. Extremely tough block polymer-based thermoplastic elastomers with strongly associated but dynamically responsive noncovalent cross-links. *Polymer* **2021**, *217*, No. 123419.
(43) Ritchie, R. O. The Conflicts between Strength and Toughness. *Nat. Mater.* **2011**, *10*, 817−822.
(44) Chen, Y.; Kushner, A. M.; Williams, G. A.; Guan, Z. Multiphase Design of Autonomic Self-Healing Thermoplastic Elastomers. *Nat. Chem.* **2012**, *4*, 467−472.
(45) Tang, Z.; Huang, J.; Guo, B.; Zhang, L.; Liu, F. Bioinspired Engineering of Sacrificial Metal-Ligand Bonds into Elastomers with Supramechanical Performance and Adaptive Recovery. *Macromolecules* **2016**, *49*, 1781−1789.
(46) Filippidi, E.; Cristiani, T. R.; Eisenbach, C. D.; Waite, J. H.; Israelachvili, J. N.; Ahn, B. K.; Valentine, M. T. Toughening Elastomers Using Mussel-Inspired Iron-Catechol Complexes. *Science* **2017**, *358*, 502−505.

https://doi.org/10.1021/acsomega.1c05609
ACS Omega 2022, 7, 2821−2830

(47) Song, Y.; Liu, Y.; Qi, T.; Li, G. L. Towards Dynamic but Supertough Healable Polymers through Biomimetic Hierarchical Hydrogen-Bonding Interactions. *Angew. Chem. Int. Ed.* **2018**, *57*, 13838−13842.
(48) Zhang, L.; Liu, Z.; Wu, X.; Guan, Q.; Chen, S.; Sun, L.; Guo, Y.; Wang, S.; Song, J.; Jeffries, E. M.; He, C.; Qing, F.; Bao, X.; You, Z. A Highly Efficient Self-Healing Elastomer with Unprecedented Mechanical Properties. *Adv. Mater.* **2019**, *31*, No. 1901402.
(49) Duan, N.; Sun, Z.; Ren, Y.; Liu, Z.; Liu, L.; Yan, F. Imidazolium-Based Ionic Polyurethanes with High Toughness, Tunable Healing Efficiency and Antibacterial Activities. *Polym. Chem.* **2020**, *11*, 867−875.
(50) Isobe, K.; Hashimoto, S.; Nozawa, A.; Kameyama, R.; Noro, A.; Kajita, T.; Matsushita, Y. Block Copolymer Composition Obtained by Modification Treatment, Method for Producing Same, Modified Block Copolymer Composition Used for Same, and Method for Producing Said Modified Block Copolymer Composition. WO2018/2076832018.
(51) Isobe, K.; Hashimoto, S.; Noro, A.; Kajita, T.; Tanaka, H.; Matsushita, Y. Block Copolymer Composition Having Ionic Group and Film. WO2019/2162412019.
(52) Rossow, T.; Seiffert, S. In *Supramolecular Polymer Networks and Gels*; Seiffert, S., Ed.; Springer International Publishing: Switzerland, 2015; Vol. *1*, pp 1−46.
(53) Guth, E. Theory of Filler Reinforcement. *J. Appl. Phys.* **1945**, *16*, 20−25.
(54) Mullins, L.; Tobin, N. R. Stress Softening in Rubber Vulcanizates. Part I. Use of a Strain Amplification Factor to Describe the Elastic Behavior of Filler-Reinforced Vulcanized Rubber. *J. Appl. Polym. Sci.* **1965**, *9*, 2993−3009.
(55) Richardson, M. O. W.; Wisheart, M. J. Review of Low-Velocity Impact Properties of Composite Materials. *Composites, Part A* **1996**, *27*, 1123−1131.
(56) Shyr, T.-W.; Pan, Y.-H. Impact Resistance and Damage Characteristics of Composite Laminates. *Compos. Struct.* **2003**, *62*, 193−203.
(57) Matadi Boumbimba, R.; Coulibaly, M.; Khabouchi, A.; Kinvi-Dossou, G.; Bonfoh, N.; Gerard, P. *Compos. Struct.* **2017**, *160*, 939−951.
(58) Yin, Z.; Hannard, F.; Barthelat, F. Impact-Resistant Nacre-like Transparent Materials. *Science* **2019**, *364*, 1260−1263.
(59) Akiba, M. Vulcanization and Crosslinking in Elastomers. *Prog. Polym. Sci.* **1997**, *22*, 475−521.
(60) Gong, J. P.; Katsuyama, Y.; Kurokawa, T.; Osada, Y. Double-Network Hydrogels with Extremely High Mechanical Strength. *Adv. Mater.* **2003**, *15*, 1155−1158.
(61) Sakai, T.; Matsunaga, T.; Yamamoto, Y.; Ito, C.; Yoshida, R.; Suzuki, S.; Sasaki, N.; Shibayama, M.; Chung, U. Design and Fabrication of a High-Strength Hydrogel with Ideally Homogeneous Network Structure from Tetrahedron-like Macromonomers. *Macromolecules* **2008**, *41*, 5379−5384.
(62) ASTM International, *Standard Test Method for Measuring the Damage Resistance of a Fiber-Reinforced Polymer Matrix Composite to a Drop-weight Impact Event*; ASTM D7136/D7136M-05; West Conshohocken, PA, 2005.
(63) Longworth, R.; Vaughan, D. J. Physical Structure of Ionomers. *Nature* **1968**, *218*, 85−87.
(64) Eisenberg, A.; Hird, B.; Moore, R. B. A New Multiplet-Cluster Model for the Morphology of Random Ionomers. *Macromolecules* **1990**, *23*, 4098−4107.
(65) Sun, T. L.; Luo, F.; Hong, W.; Cui, K.; Huang, Y.; Zhang, H. J.; King, D. R.; Kurokawa, T.; Nakajima, T.; Gong, J. P. Bulk Energy Dissipation Mechanism for the Fracture of Tough and Self-Healing Hydrogels. *Macromolecules* **2017**, *50*, 2923−2931.
(66) Du, C.; Zhang, X. N.; Sun, T. L.; Du, M.; Zheng, Q.; Wu, Z. L. Hydrogen-Bond Association-Mediated Dynamics and Viscoelastic Properties of Tough Supramolecular Hydrogels. *Macromolecules* **2021**, *54*, 4313−4325.
(67) Zhu, C. N.; Zheng, S. Y.; Qiu, H. N.; Du, C.; Du, M.; Wu, Z. L.; Zheng, Q. Plastic-Like Supramolecular Hydrogels with Polyelectrolyte/Surfactant Complexes as Physical Cross-links. *Macromolecules* **2021**, *54*, 8052−8066.
(68) Qu, M.; Deng, F.; Kalkhoran, S. M.; Gouldstone, A.; Robisson, A.; Van Vliet, K. J. Nanoscale Visualization and Multiscale Mechanical Implications of Bound Rubber Interphases in Rubber−Carbon Black Nanocomposites. *Soft Matter* **2011**, *7*, 1066−1077.
(69) Sutherland, L. S.; Guedes Soares, C. Impact Characterisation of Low Fibre-Volume Glass Reinforced Polyester Circular Laminated Plates. *Int. J. Impact Eng.* **2005**, *31*, 1−23.
(70) Hosseinzadeh, R.; Shokrieh, M. M.; Lessard, L. Damage Behavior of Fiber Reinforced Composite Plates Subjected to Drop Weight Impacts. *Compos. Sci. Technol.* **2006**, *66*, 61−68.
(71) Liu, H.; Chen, F.; Liu, B.; Estep, G.; Zhang, J. Super Toughened Poly(Lactic Acid) Ternary Blends by Simultaneous Dynamic Vulcanization and Interfacial Compatibilization. *Macromolecules* **2010**, *43*, 6058−6066.
(72) Spencer, M. W.; Wetzel, M. D.; Troeltzsch, C.; Paul, D. R. Effects of Acid Neutralization on the Properties of K^+ and Na^+ poly(Ethylene-Co-Methacrylic Acid) Ionomers. *Polymer* **2012**, *53*, 569−580.
(73) Lee, J.-H.; Veysset, D.; Singer, J. P.; Retsch, M.; Saini, G.; Pezeril, T.; Nelson, K. A.; Thomas, E. L. High Strain Rate Deformation of Layered Nanocomposites. *Nat. Commun.* **2012**, *3*, No. 1164.
(74) Wang, C.; Roy, A.; Chen, Z.; Silberschmidt, V. V. Braided Textile Composites for Sports Protection: Energy Absorption and Delamination in Impact Modelling. *Mater. Des.* **2017**, *136*, 258−269.

https://doi.org/10.1021/acsomega.1c05609
ACS Omega 2022, 7, 2821−2830